AIMS Geosciences, 3 (1): 116-141
DOI: 10.3934/geosci.2017.1.116
Received date 19 September 2016
Accepted date 13 April 2017
Published date 19 April 2017

http://www.aimspress.com/journal/geosciences

Research article

Landslide Susceptibility Mapping Using GIS-based Vector Grid File (VGF) Validating with InSAR Techniques: Three Gorges, Yangtze River (China)

Cem Kıncal [1,*], Zhenhong Li [2], Jane Drummond [3], Peng Liu [4], Trevor Hoey [3] and Jan-Peter Muller [5]

[1] Geological Engineering Department, Engineering Faculty, Dokuz Eylül University, Izmir, Turkey
[2] School of Civil Engineering and Geosciences, Newcastle University, Newcastle upon Tyne, UK
[3] School of Geographical and Earth Sciences, University of Glasgow, Glasgow G12 8QQ, UK
[4] Southern University of Science and Technology, Nanshan District, Shenzhen, Guangdong, China
[5] Mullard Space Science Laboratory, Department of Space and Climate Physics, University College London, UK

*** Correspondence:** Email: cemkincal@gmail.com

Abstract: A landslide susceptibility assessment for the Three Gorges (TG) region (China) was performed in a Geographical Information System (GIS) environment and Persistent Scatterer (PS) InSAR derived displacements were used for validation purposes. Badong County of TG was chosen as case study field. Landslide parameters were derived from two datasets. The Advanced Spaceborne Thermal Emission and Reflection Radiometer (ASTER) Global Digital Elevation Map (GDEM) was used to calculate slope geometry parameters (slope, aspect, drainage, and lineament), while geology and vegetation cover were obtained from Landsat and ASTER data. The majority of historical landslides occurred in the sandstone-shale-claystone intercalations. It appears that slope gradients are more critical than other parameters such as aspect and drainage. The susceptibility assessment was based on a summation of assigned susceptibility scores (points) for each 30×30 m

unit in a database of a Vector Grid File (VGF) composed of 'vector pixels'. A landslide susceptibility map (LSM) was generated using VGF and classified with low, moderate and high landslide susceptibility zones. The comparison between the LSM and PS InSAR derived displacements suggests that landslides only account for parts of the observed surface movements.

Keywords: ASTER GDEM; PS InSAR; Three Gorges; landslide susceptibility

1. Introduction

Landslides are natural processes that can be triggered directly or indirectly by natural and/or human activities. Natural activities include high rainfall, earthquakes and volcanic eruptions [1], and human activities include land-use change, deforestation, excavation, change in the slope profile, and irrigation [2]. Indirect effects could result from changes in rainfall associated with an increase in surface water area. Landslides are devastating to human activities, thus predicting their occurrence and effect is critical. An established tool for this is Landslide Risk Maps (LRMs). LRMs is an outcome of Landslide Hazard Maps (LHMs), but producing both LRMs and LHMs requires information which may be difficult to obtain (such as detailed geological maps, landslide inventory maps, historical records, rainfall records and earthquake magnitudes). A practical alternate is a Landslide Susceptibility Map (LSMs).

LSMs map potential landslide areas [3]. Landslide susceptibility is determined by several related, spatially-distributed factors (e.g. geology, slope angle, slope aspect, drainage, etc.), pertinent to instability. The landslide susceptibility of any area has usually been categorized in the range "stable to unstable", thus indicating landslide-prone areas [4,5].

In 1979, an early form of LSMs at the scale 1:125.000, was prepared of the San Francisco Bay region according to slope units, rock lithologies, susceptible bedrock, susceptible superficial deposits and landslide deposits [6]. Nilsen and Wright combined slope angle and rock lithology categories and classified the region into five areas: (1) stable, (2) generally stable, (3) moderately stable, (4) moderately unstable, and (5) unstable [3]. In general, various approaches have been developed to evaluate landslide susceptibility [7] and landslide hazard for the regional scale (e.g. river basin) [8–11].

Brabb circulated a questionnaire to international experts concerning the availability of landslide inventory maps to celebrate the start of the International Decade of Reduction of Natural Hazards (1991–2000) [12]. The result showed that most countries had landslide inventory maps with national coverage at less than 25% except Austria, Hungary, Korea, Taiwan, Hong Kong, New Zealand, Canada and Costa Rica [3].

Later, geoscientists in many countries started preparing landslide maps with the help of GIS [13–15]. Up to now, many research and educational institutes and commercial companies have been offering information on geological hazards, particularly landslides. This arises from a

widespread application of GIS and remote sensing techniques. Emergence of GIS applications in landslide map generation is critical by this time.

Various studies have been conducted on landslide susceptibility mapping [1,4,6,8,15–22]. A rating was determined taking into account the ratio of the total aspect and slope of topography and the aspect and slope of topography per grid interval where the landslide occurred in the Janghung area of South Korea. Finally, the rating was summed to calculate the landslide susceptibility index (LSI) per grid cell [16,17]. Colorado State University proposed debris flow hazard susceptibility mapping at a scale 1:24.000, prepared using an algorithm taking into account the influence of factors such as slope angle, slope orientation, Unified Soil Classification System (USCS), clay content and clay's geotechnical and erosive properties [23]. With the help of a raster GIS, [24] used a weighting factor procedure to produce a landslide susceptibility map (LSM) in the Wondogenet area in the eastern Ethiopian rift. Landslide susceptibility assessments were performed using landslide occurrence data, and layers representing lithology, drainage network, geology, slope angle, slope aspect and vegetation cover. Weightings were assigned with regard to the observed landslide intensities for each class, resulting in LSMs. In this case, a landslide hazard map was subsequently created by overlaying the susceptibility maps; the values of each grid cell in the contributing layers were summed and divided by the total number of controlling parameters [3]. Zhu et al. integrated human expertise on landslide-environment relationships with GIS under fuzzy logic. Geology, slope and strata, slope gradient, relative relief and slope shape were used as rule set to conduct landslide susceptibility in Three Gorges area (China) [25]. Authors validated their analysis by examining the usefulness of the fuzzy membership values. They used 21 landslides and the computed fuzzy membership value for susceptibility at each site was obtained from the derived fuzzy membership map.

In recent decades, several studies on landslide susceptibility mapping have been carried out in Italy. Orthophotos of southern Italy were used to determine landslide areas to form landslide inventory maps [21]. Magliulo et al. used lithology, landuse, slope gradient and aspect to prepare LSMs. These LSMs compared well with a geomorphological map. To obtain a LSM, a landslide occurrence map is required to evaluate landslide related data statistically. An occurrence map is used together with data such as geology, slope, aspect, drainage, etc. to determine potential landslide sites which have the same conditions as those on the occurrence map. Landslide susceptibility analysis requires a large amount of data as input, thus making high budgetary and time demands [20]. Kıncal et al. carried out landslide susceptibility assessment in Izmir city (Turkey) using the variables of lithology, slope gradient, slope aspect, distance to drainage, distance to roads and distance to fault lines in logistics regression analysis. Lithology played the most important role in determining landslide occurrence and distribution on the basis of the provided coefficients [26].

Bai et al. prepared a detailed landslide susceptibility map in the Zhongxian segment in the Three Gorges area of China using logistic regression method with the help of Geographical Information Systems (GIS). Statistical relationships for landslide susceptibility were conducted using landslide and landslide triggering factors [27]. Seed cells were used to be dependent

variable in order to create a reliable logistic regression model. The seed cells were formed from landslide boundaries and represented the pre-failure undisturbed morphological conditions. Yilmaz et al. [used statistical index (Wi) method of Van Westen to conduct landslide susceptibility in Devrek (Zonguldak/Turkey) [28,29]. Ten parameters of elevation, slope, aspect, profile curvature, plan curvature, distance to streams, drainage density, distance to ridges, distance to road and power line network, and lithology were used during the analyses. Seed cells of Süzen and Doyuran were used to define decision rules of slope instabilities and percentile class divisions [30]. In all data sets authors used, elevation, lithology, slope aspect and drainage density were found as critical parameters for landslide occurrence. Chen et al. prepared a landslide susceptibility map in the Zigui segment of the Three Gorges area of China by using light detection and ranging (LiDAR) and logistic regression model (LRM) [31]. After processing LiDAR & DMC data and geological maps and landslide-controlling factors were derived as landslide density, digital elevation model (DEM), slope angle, aspect, lithology, land use and distance from drainage. The likelihood ratio (LR) analysis then applied to find correlation between the landslide locations and landslide-controlling factors. Logistic Regression Model (LRM) was used to predict the occurrence of landslides. Wu et al. used rough sets and back-propagation neural networks (BPNNs) to map landslide susceptibility on the Zigui-Badong of the Three Gorges area [32]. Landslide inventory map was prepared with the help of field works. Twenty-two landslide related parameters were created using topographical and geological maps, Landsat ETM+ and HJ-A satellite images. Elevation, slope, profile curvature, catchment aspect, catchment height, distance from drainage, engineering rock group, distance from faults, slope structure, land cover, topographic wetness index, and normalized difference vegetation index were used as independent variables set by the rough set and correlation coefficient analysis. Three layered and four layered BPNN were trained and used to obtain landslide susceptibility map. Kavzaoglu et al. prepared nine thematic maps associated with lithology, slope, aspect, land cover, drainage density, topographic wetness index, elevation, slope length and distance to road to create landslide susceptibility map with the help of multi-criteria decision analyses (MCDA) and support vector regression (SVR) methods for the province of Trabzon (Turkey) [33]. Performances of the methods were compared with logistic regression model. Tehrany et al. used weights-of-evidence (WoE) model to assess the impact of classes of each conditioning factor on flooding through bivariate statistical analysis (BSA) [34]. Their WoE model was integrated with SVM in order to enhance the performance of each method. Also, increasing the accuracy of the flood susceptibility map to properly manage the prone area of the floods, is aimed. Wu et al. used object based data mining methods were applied to a case study of landslide susceptibility assessment on the Guojiaba Town of the Three Gorges area [35]. Eleven landslide related factors were extracted using satellite images, topographical and geological maps. These factors were calculated as independent variables using significance testing and correlation coefficient analysis including slope, profile curvature, engineering rock group, slope structure, distance from faults, land cover, tasselled cap transformation wetness index, reservoir water level, homogeneity, and first and second principal

components of the images. Decision tree and SVM models were used to prepare landslide susceptibility map. Du et al. used support vector machine (SVM) to produce landslide susceptibility maps for the Daguan County of Zhaotong City (Yunnan Province/China) [36]. Landslide conditioning parameters of slope angle, slope aspect, altitude, distance to faults, distance to rivers, and distance to roads, NDVI, rainfall and lithology were used during the analysis. SVM model was validated by using area under the curve (AUC) methods. The validation results authors obtained showed high accuracy (84.73%).

In this paper, we present a landslide susceptibility map as a case study for the Badong County in Three Gorges (TG) region of China to use geology, slope aspect, slope angle, drainage network, lineament and vegetation cover data from Landsat imagery, ASTER imagery and a GDEM to create a Vector Grid File (VGF) (= Vector pixel) based GIS model. Then, we compare this VGF-based LSM with the deformation signals derived using Persistent Scatter Interferometric Synthetic Aperture Radar (PS InSAR).

2. Study Area

The study area, located in the TG region (China, Figure 1), is well known for its dam construction. The TG dam is the largest water management project in the world today. The total catchment area of TG project is about 1.0×10^6 km^2 with 4.5×10^{11} m^3 the average annual runoff [37]. It is claimed that the main functions of the TG dam include flood control and hydro-electric power. This dam is the most important flood control project built on the Yangtze River. The flood season of the Yangtze River is between June and September during which 70% to 75% of the total annual rainfall occurs. Historical records show that 214 floods occurred in the Yangtze Valley between the beginning of the Han Dynasty (206 B.C.) and the end of the Qing Dynasty (1911 A.D.), i.e. about one per decade [38]. Since the 1920s, flood hazards have threatened more than 1.5 million ha of crops, 15 million people and their properties and railway transportation. The normal water level and the total storage capacity of the dam are 175 m and 3.93×10^{10} m^3, respectively. The water level is reduced to 145 m to control any harmful effects of floods on the dam structure.

There are frequent precipitation-related hazards in the TG region. More than 30,000 people died in a huge flood on the Yangtze in 1954, in which 90 percent of the 30,000 deaths were disease related [40]. At least 2,000 km^2 of farm land were flooded and more than 1,500 people lost their lives because of the flood in 1998 [41]. In 2008, heavy precipitation led to serious storm and flood disasters such as the collapse or flooding of rural homes, destruction of cropland, heavy loss of livestock and poultry farms and damage to urban and rural roads [42]. Other frequent natural hazards in this region are geological disasters, such as landslides and mud flows. It was reported that 34 counties in Chongqing had suffered from collapse, landslide and rock and mud flow [43]. The impounding of the TG dam reservoir was started on April 1, 2003 [37]. From this time, the water level of the Yangtze River rose and TG Dam Lake was created. Landsat images can be used to display water level change from 2000 to 2006 (Figure 2).

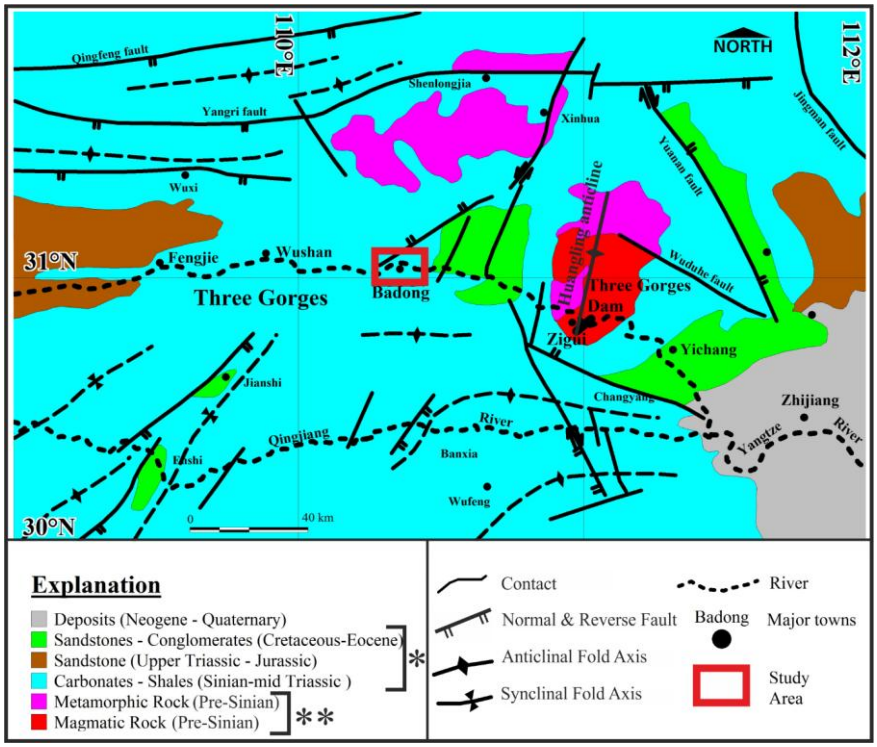

Figure 1. Geology and tectonic setting map of Three Gorges region (Modified from [39]) (: Presinian crystalline basement, * : Sinian-Eocene sedimentary cover series).**

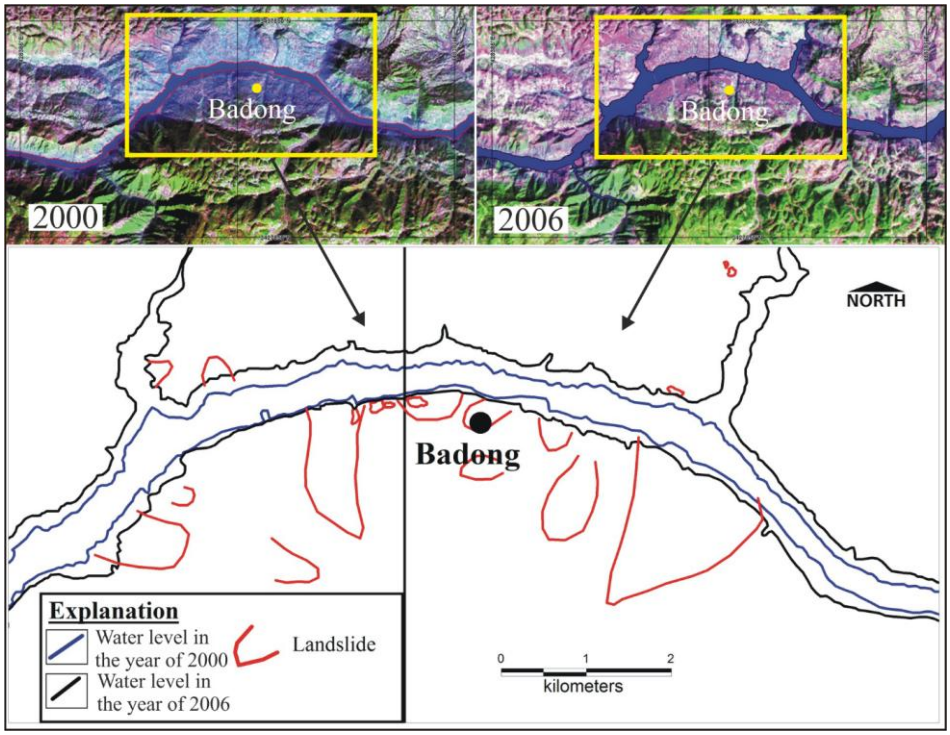

Figure 2. Water level change in the Yangtze River in the years 2000 and 2006. (Locations of the large landslides were extracted from [44]).

Many landslides occurred near the water level of the Yangtze River and more than 97% of landslides were on the main channel of the TG region (Figure 2 and 3). Some landslides, such as those in Wanxian County where is nearly 190 km far from the study area in the southwest-west direction, occurred at different elevation ranges and with sliding surfaces following the nearly horizontal rock stratums (Figure 3) [45]. Slope instabilities already threaten several new towns and the rising water level in the reservoir has the potential to trigger old instabilities as well as create new ones [39].

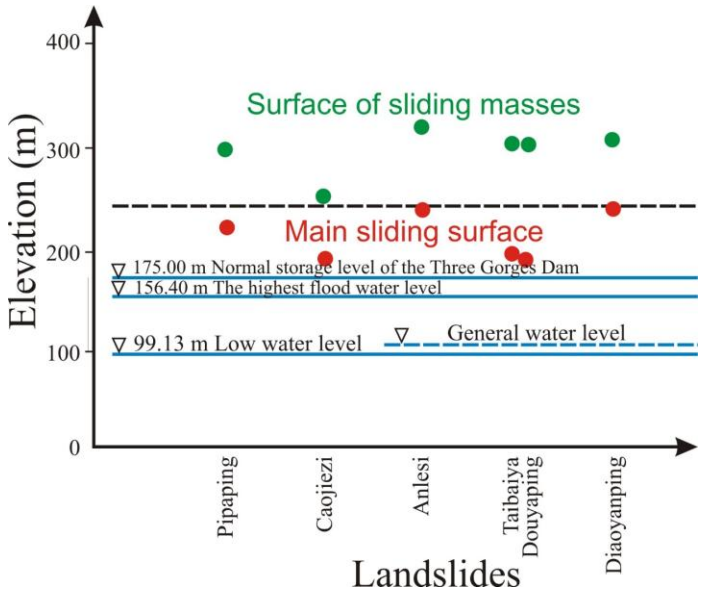

Figure 3. Elevation ranges of the old landslides that have occurred in Wanxian County (modified from [42]).

A field trip was carried out in the Badong County to check surface movements and cracks have occurred on the man-made structures (Figure 4). This field work showed that landslides in the area are still active. Cracks were recorded on some roads which were built in 2006 and 2007.

Figure 4. (a) A view of surface cracks seen in a landslide field in Badong County; (b) Surface displacements observed in a landslide field in Badong County.

The geological setting of the area consists of two major formations, a Pre-Sinian crystalline basement and a Sinian-Eocene sedimentary cover series (Carbonates, shales, sandstones and conglomerates) (modified from [46]). The crystalline basement is composed of metamorphic and magmatic rocks and the sedimentary cover is composed of interbedded sandstone, shale and claystone intercalations.

The Huangling anticline is the major folding system in the area. It is 50 km in length, lying to the southeast of Zigui, with Pre-Sinian metamorphic and magmatic rocks forming the fold's core [39]. The reason for building the TG Dam in its present location is the strength and stability of this anticlinal structure and the lack of any significant earthquakes in this area [37] (Figure 1).

The southern Zigui and Badong area is characterised by secondary faults, consistent with the ENE–WSW oriented fold system [47]. Weak zones were formed by the secondary fault and fracture systems which trigger slope instability.

3. Datasets Used in This Study

A detailed investigation has been performed mainly involving remotely sensed Landsat ETM+ and ASTER images, SAR interferometric processing, LSM and validation. PS InSAR data was used to validate analyses performed. Our GIS-model is based on the information provided by ASTER and Landsat TM and ETM+ images, ASTER GDEM data, published literature and limited field observations.

3.1. ASTER Optical Imagery

Data from the NASA Earth Observing System (EOS) satellite-based instruments offer many resources for collecting high spatial and temporal resolution information related to urban and non urban areas. ASTER on board the Terra platform is well-suited for geological analysis [48]. The ASTER instrument was built by Japan's Ministry of Economy, Trade and Industry (METI) and launched onboard the NASA's Terra spacecraft in December 1999. It has an along-track stereoscopic capability using its infrared spectral bands and its nadir-viewing and backward-viewing telescopes to acquire stereo images with a base-to-height ratio of 0.6. One nadir-looking ASTER Very Near Infrared (VNIR) scene consists of 4,100 samples by 4,200 lines [49]. ASTER data can be used for analysing and investigating urban land cover/land-use and biophysical parameters such as biomass, spatial metrics and surface temperature/emissivity [50–52]. In this study, two Terra ASTER Level 1A images acquired on July 17, 2000 and September 25, 2002 were used.

3.2. Landsat Optical Imagery

The Landsat Thematic Mapper (TM), a sensor carried onboard Landsats 4 and 5, has acquired images of the Earth from July 1982. The temporal resolution of TM is sixteen days [53]. Landsat 7

was launched on April 5, 1999. The Earth observing instrument on Landsat 7, the Enhanced Thematic Mapper Plus (ETM+), extends the capabilities of the highly successful Thematic Mapper instruments on Landsat 4 and 5 [54]. The scene size is 170 km in the north-south and 183 km in the east-west directions. Landsat images have been resampled using cubic convolution (CC). Four Landsat images acquired on April 17, 1987, May 14, 2000, November 6, 2000 and September 12, 2006 were used in this study (Table 1). Landsat images were used in this study to map water level changes of the Yangtze River and prepare geological and vegetation maps.

In this study, geological boundaries were visually interpreted using Landsat TM 7-3-1, 7-4-1 and ETM+ 7-3-1 and 7-4-2 data. Screen digitisation was performed during the preparation of a geological map. ASTER band combinations of different channels 3-2-1, 4-6-9 and 4-6-12 images were then employed to correct some contacts of the formations (Figures 5 and 6). Details of the satellite images are given in Table 1.

Table 1. Landsat and ASTER images used in this study.

Acquire Date	Dataset	Cloud cover (%)	Path/Row	Number of Bands	Spatial resolution	Cover area (km)
1987-04-17	Landsat TM	0	125/39	7	Band 6=120 m Other bands=30 m	170×183
2006-09-12	Landsat TM	0	125/39	7		
2000-05-14	Landsat ETM+	0	125/39	8	Band 6L=60 m Band 8=15 m Other bands=30 m	
2000-11-06	Landsat ETM+	0	125/39	8		
2000-07-17	ASTER	3	125/39	14	Bands 1, 2, 3N and 3B= 15 m Bands 4-9=30 m Bands 10-14=90 m	60×60
2002-09-25	ASTER	5	125/39	14		

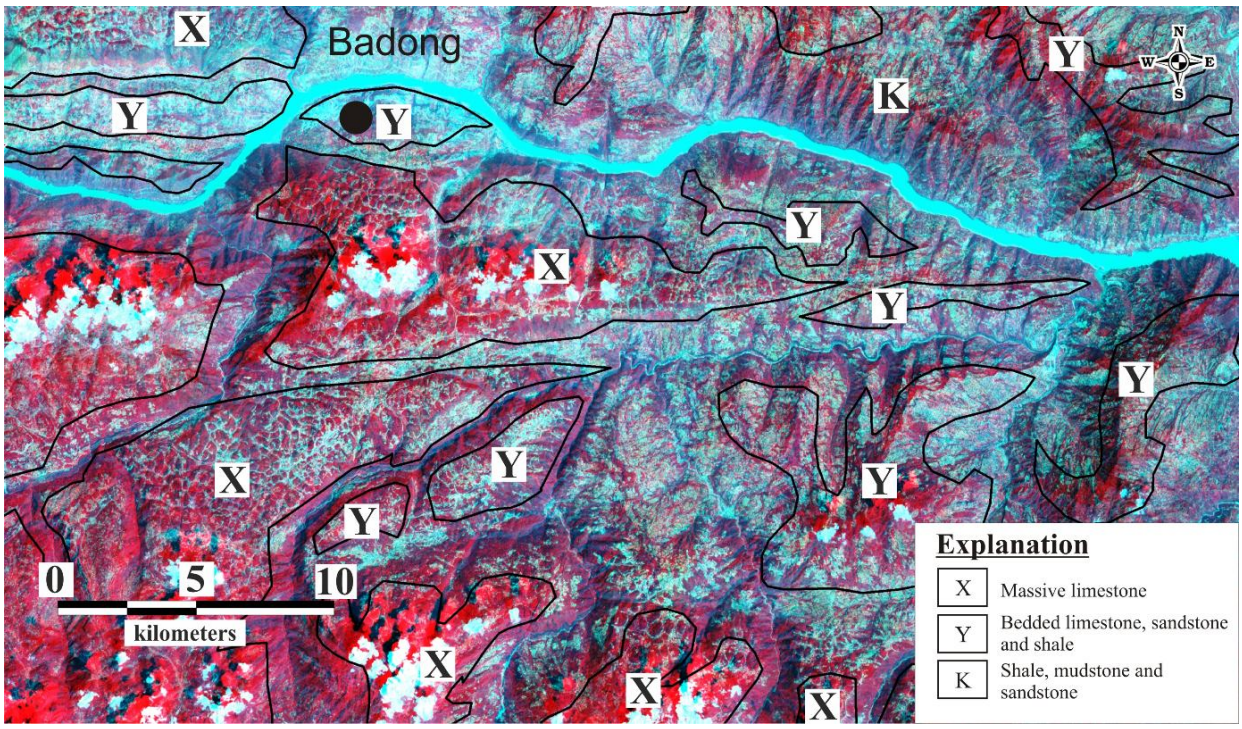

Figure 5. ASTER 321 false color composite view of the study area (The ASTER image was acquired in 25th of September, 2002).

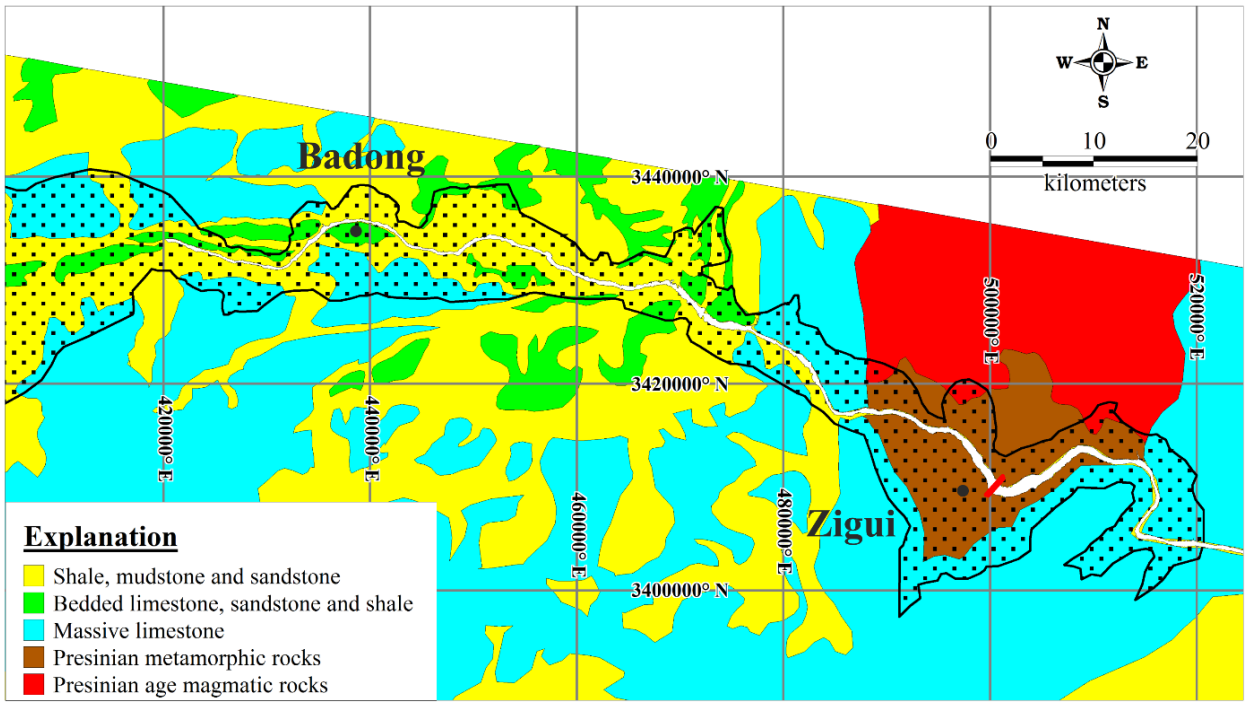

Figure 6. Geological map of the Three Gorges Project area extracted from Landsat TM/ETM+ and ASTER images.

3.3. ASTER GDEM

ASTER GDEM (Version 1) was used in this study to prepare the maps of slope angle, slope aspect, drainage, and lineament.

Independent research was conducted using GPS survey benchmarks to assess the absolute vertical accuracy of ASTER GDEM in different geographical regions over China [55]. In the TG region, the coordinates of 121 GPS survey stations were obtained with centimetre level accuracy (Figure 7.a), and then a correlation analysis between GPS and ASTER GDEM was performed. A correlation of 0.97, a mean difference of -5.9 metres and a RMS value of 12.1 metres were observed [56] (Figure 7.b).

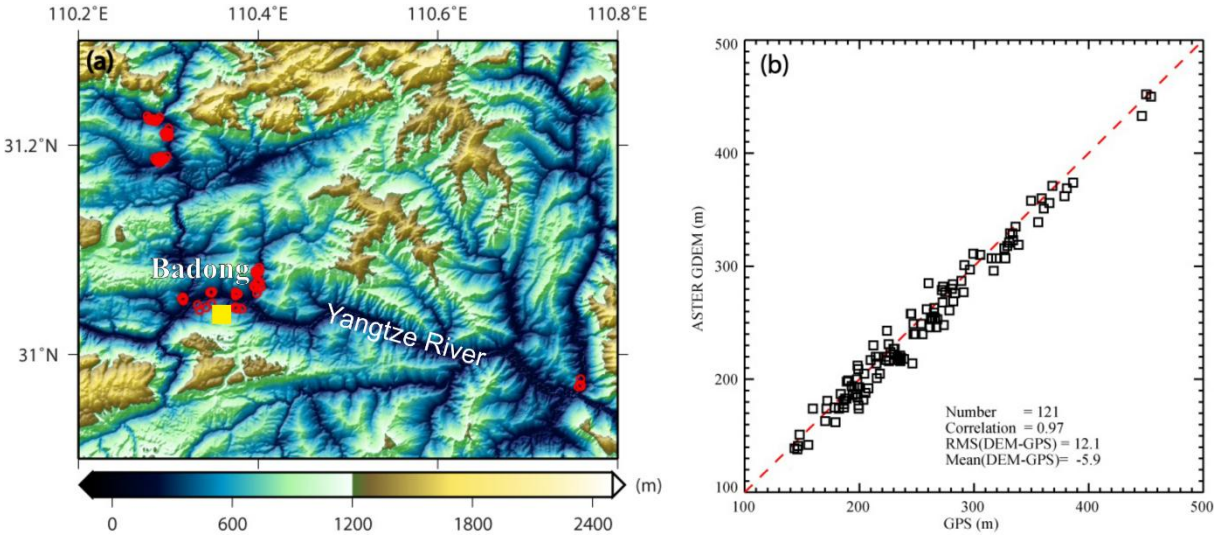

Figure 7. (a) Shaded relief map of the study area in Three Gorges with the locations of Static GPS points plotted on the ASTER GDEM. Red circles represent GCPs. (b) Scatterplot of ASTER GDEM and Static GPS heights in Three Gorges. The dashed line represents the line of perfect fit [55].

4. **Methods**

Methods can be divided into six stages: (i) determination of variables relevant to landslide susceptibility; (ii) preparation of thematic maps using variables, (iii) extraction of spatial information to generate a Vector Grid File (VGF) having 30 x 30 metres resolution, (iv) preparation of a LSM using the VGF and (v) preparation of a thematic deformation map using Persistent Scatterer (PS) InSAR techniques and (vi) a comparison of (iv) and (v) (Figure 8).

After visual interpretation of Landsat and ASTER images to extract geological outcrop boundaries in the study area, these outcrops were regrouped based on lithological attributes rather than their stratigraphic content and age [18, 30]. Many researchers involve lithology as a factor in

susceptibility mapping [57–63]. Vector Grid File (VGF) based GIS model was created to determine the LSM for the Three Gorges, Yangtze River (China) site. Then, this LS map is validated with InSAR results.

Researchers working on soils obtained from different landslide sites in TG area have found that the average internal friction angle for saturated soils is 10 degrees [64]. A slope angle map was thus categorized in classes 0–10°, 11–20°, 21–30°, 31–40° and > 40° as having low (for 0–10°), moderate (for 11–20° and 21–30°) and high landslide susceptibility (for 31–40° and >40°) (Table 3, Figure 9).

An aspect hazard map was prepared according to whether the aspect of the slope inclined towards the Yangtze River. This aspect map was classified into 8 classes according to aspect directions of 0–45°, 45–90°, 90–135°, 135–180°, 180–225°, 225–270°, 270–315° and 315–360°. For the southern slopes of the Yangtze River, an aspect zone of 315–45° was chosen and for the northern slopes of the Yangtze River, an aspect zone of 135–225° was chosen as the critical aspect zones for landslides (Figure 8 and 9).

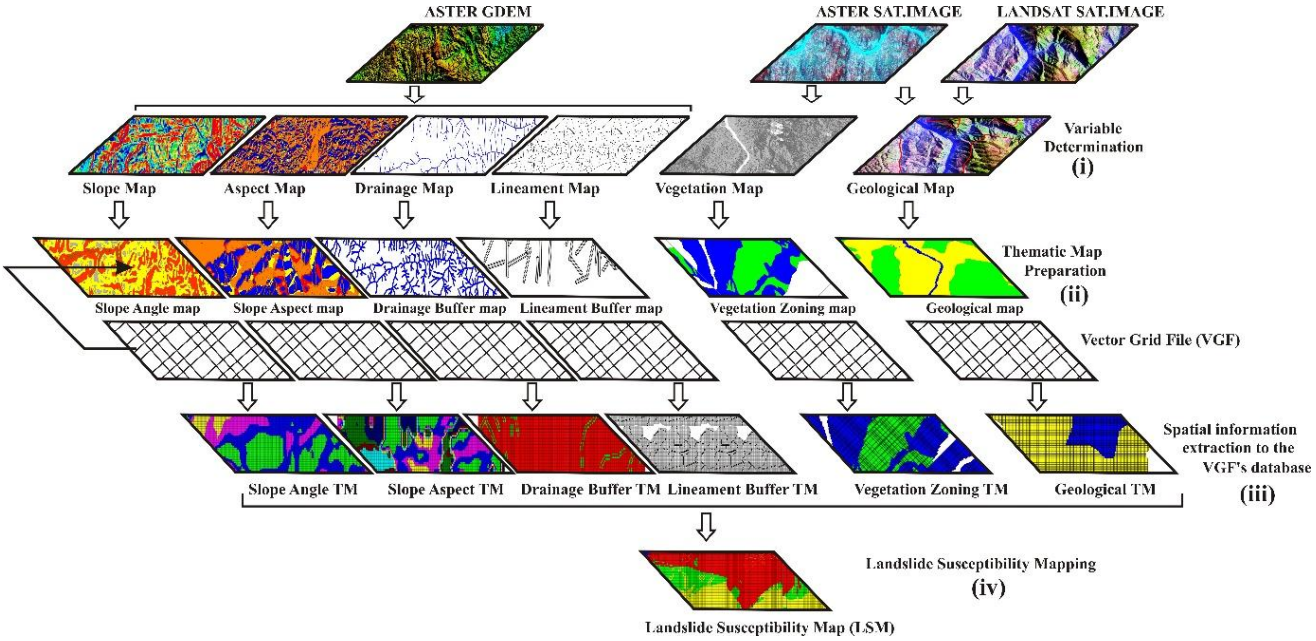

Figure 8. The processing of the data-sets used to obtain LSM. Flow chart of the study ((i) determination of variables relevant to landslide susceptibility; (ii) preparation of thematic maps using variables, (iii) extraction of spatial information to generate a Vector Grid File (VGF) having 30 x 30 metres resolution, (iv) preparation of a LSM using the VGF and (v) preparation of a thematic deformation map using Persistent Scatterer (PS) InSAR techniques).

Lineaments were digitised as geological structures. The distance to the lineament map (lineament buffer map) signifies the presence of joint-fractures affecting shear strength [18,30]. Buffer zones were created for distances of 0–50, 50–100 and 100–200 metres for each lineament feature (Figure 8).

The drainage network was digitized from generated contours using ASTER G-DEM data [65]. After digitising, buffer zones were created at 0–50, 50–100 and 100–200 metres for each drainage channel (Figure 9b). Also, water level in 2006 digitized from a Landsat image, was considered during the drainage buffer analysis, as later described.

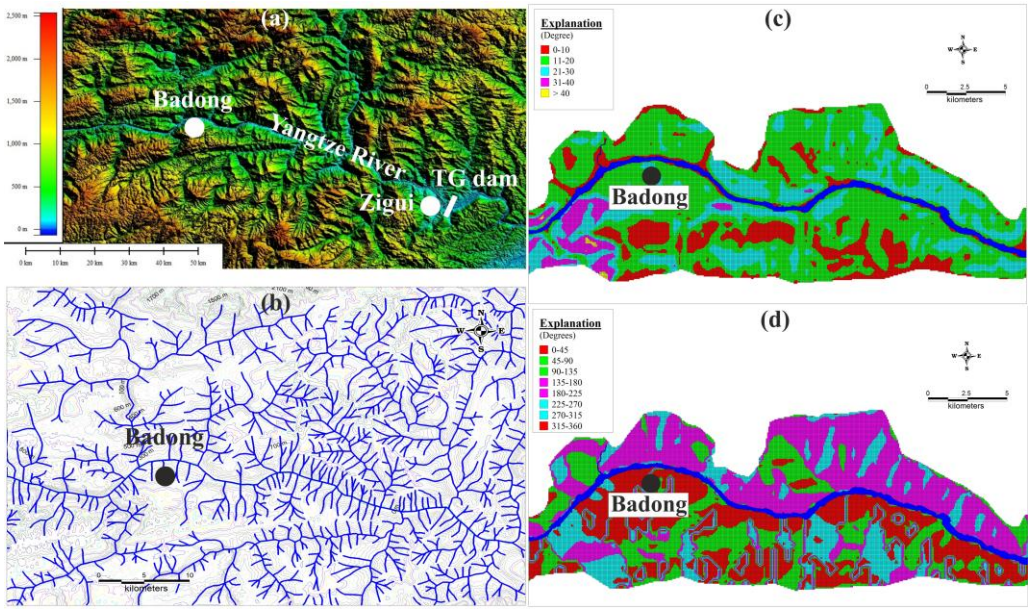

Figure 9. (a) ASTER GDEM of the study area, (b) Vector drainage network of the study area (c) Slope angle map of the Badong County, (d) Aspect map of the Badong County.

A vegetation map was prepared using the Normalized Difference Vegetation Index (NDVI) calculation in the range between -1 and 1. Forest, agricultural fields, barren land, water and wet areas are the main land cover classes determined from this image. The NDVI map was classified as water (-1.00 to -0.01), wet areas (0.00 to 0.32), barren land (0.33 to 0.63), intermediate vegetation (0.64 to 0.76) and dense vegetation (0.77 to 1.00). A high susceptibility score was given to barren land and a low score to forested land.

In an approach developed by [66], spatial information for all map layers saved in a database related to landslide potential was produced. An overlay technique was used to combine data from a number of maps in order to prepare a new map that is termed a "VGF-based LSM". For the preparation of the susceptibility map, raster background images (e.g. geological maps derived from satellite imagery) were digitized to form geology layers. Then, all digital thematic maps (geology, slope angle, slope aspect, drainage, lineament, vegetation) were converted to vector pixels from a dataset of all digital maps [66]. GIS enables end users to carry out a complete land-use planning and seismic-risk assessment at regional, sub-regional and local scales [67]. All analyses for the present study were carried out at a sub-regional scale.

A Vector Grid File (VGF), containing 132.692 vector areas (or "vector pixels") of size 30×30 m was created using the "Grid Maker" command (of MapInfo Professional) to cover the Badong

County (see Figure 10). Then, columns were inserted into the VGF file's attribute database – one for each digital raster map. Next, each digital thematic map was overlaid on the new blank VGF.

A susceptibility score was assigned to the database for each map pixel as suggested by [24] and [68] (Table 3). Then the VGF susceptibility score was calculated according to Equation (1)

$$\text{Landslide Susceptibility} = \sum \text{Points of } [\text{San} + \text{Sas} + \text{Lit} + \text{Lin} + \text{Dra} + \text{Veg}] \quad \ldots\ldots\ldots\ldots 1$$

where;

San: Slope Angle, Sas: Slope Aspect, Lit: Lithology, Lin: Lineament, Dra: Drainage, Veg: Vegetation.

A LSM was prepared using the total number of VGF susceptibility points (scores) (Figure 11). The LSM has been obtained by reclassifying the values obtained by means of Eq. (1) into three categories: High, Medium and Low.

A deformation map was then created using PS InSAR results. The prepared LSM and the PS InSAR deformation results are compared in Section 6.

Table 2. Details of variables used to prepare landslide susceptibility map.

Variable	Data Source	Techniques used	Data Type
Geology	Landsat and ASTER images	Visual interpretation	Polygon
Slope angle	ASTER GDEM	Contouring	Polygon
Slope Aspect	ASTER GDEM	Contouring	Polygon
Lineament	Ortorectified Landsat & ASTER images	Screen digitising	Polyline
Drainage	ASTER GDEM	Screen digitising	Polyline
Vegetation	Landsat	NDVI	Polygon

NDVI: Normalized Difference Vegetation Index

5. Landslide Susceptibility Analysis

LSMs are a special type of engineering geological maps, and present all the components of the geological and geo-morphological environment. Such maps should be based on the combination of all relevant – mainly engineering geological – parameters. This combination can be realized by using an overlay process in the GIS environment, which is perhaps one of the key functions of a GIS; it allows for construction of a new integrating layer [69]. One can distinguish three major categories of approaches to GIS-based land-use suitability analysis in the literature: (1) computer-assisted overlay mapping, (2) multi-criteria evaluation methods, and (3) soft computing or geo-computation methods [70]. Overlay with a weighting technique was used during the landslide susceptibility analysis. Point scores were assigned according to sliding susceptibilities as defined in Table 3 and 4. If the unit cell in the VGF is more susceptible to sliding, then a high point (score) is given, otherwise a low one is assigned [71,72]. Categories (1) and (2) are performed in this study as other scientists did. But, different point scores to the areas which have different type of susceptibility class are given in this study and VGF-

based technique is a novel in this case study area. For this purpose, the existing landslide inventory map of the study area was used in order to perform a zonation of land units similarly prone to generate landslides or in order to quantitatively validate the obtained susceptibility map.

Table 3. Points (scores) assigned to each vector pixels of VGF depending on susceptibility factors.

Geology/lithology Category	**Lithology Points**	**Slope Aspect Category**	**Slope Aspect Points**
Sandstone-shale-claystone intercalations	30	0-45°	20
Bedded limestone and sandtone	10	45-90°	10
Massive limestone	10	90-135°	10
Presinian metamorphic rock	10	135-180°	20
Presinian magmatic rock	10	180-225°	20
Vegetation Category	**Vegetation Points**	225-270°	10
No	10	270-315°	10
Intermediate	10	315-360°	20
Dense	0		
Lineament Category	**Lineament Points**	**Drainage Category**	**Drainage Points**
In 50 m buffer	5	In 50 m buffer	5
In 50-100 m buffer	10	In 50-100 m buffer	10
In 100-200 m buffer	15	In 100-200 m buffer	15
Slope Angle Category	**Slope Angle Points**		
0-10°	10		
11-20°	20		
21-30°	20		
31-40°	30		
> 40°	30		

There is no doubt that landslides will be seen along the slopes of the Yangtze River. Slope angle and slope aspect maps were prepared to determine landslide susceptibility analysis zones (Figure 10). As already stated, the vector grid file (VGF) is made up of 132,697 cells (Figure 10) with the dimension of each cell being 30 x 30 m (Table 3 and 4).

Table 4. Database example. Vector grid layer created using geology, slope angle, slope aspect, drainage, lineament and vegetation cover maps for fifteen vector pixels (LQ177-LQ188).

Vektor pixel coordinate	Vektor pixel column id	Vektor pixel row number	Slope _min	Slope _max	Score of the slope	Aspect _min	Aspect _max	Score of the aspect	Lithology	Score of the Lithology	Score of the Lineament _50m	Score of the Lineament _100m	Score of the Lineament _200m
LQ177	LQ	177	10	20	20	225	270	10	seyl and sandstone	30	0	0	0
LQ178	LQ	178	10	20	20	225	270	10	seyl and sandstone	30	0	0	0
LQ179	LQ	179	10	20	20	225	270	10	seyl and sandstone	30	0	0	0
LQ180	LQ	180	10	20	20	225	270	10	seyl and sandstone	30	0	0	0
LQ181	LQ	181	10	20	20	225	270	10	seyl and sandstone	30	0	0	0
LQ182	LQ	182	10	20	20	225	270	10	seyl and sandstone	30	0	0	0
LQ183	LQ	183	10	20	20	225	270	10	seyl and sandstone	30	0	0	0
LQ184	LQ	184	10	20	20	225	270	10	seyl and sandstone	30	0	0	0
LQ185	LQ	185	10	20	20	225	270	10	seyl and sandstone	30	0	0	0
LQ186	LQ	186	10	20	20	225	270	10	seyl and sandstone	30	0	0	0
LQ187	LQ	187	10	20	20	225	270	10	seyl and sandstone	30	0	0	0
LQ188	LQ	188	10	20	20	180	225	20	seyl and sandstone	30	0	0	0

Score of the Stream_50m	Score of the Stream_100m	Score of the Stream_200m	Score of the Vegetation	TOTAL SCORE
0	0	0	10	70
0	0	0	10	70
0	0	0	10	70
0	0	0	10	70
0	0	0	10	70
0	0	0	10	70
0	0	0	10	70
0	0	0	10	70
0	0	0	10	70
0	0	0	10	70
0	0	0	10	70
0	0	0	10	70
0	0	0	10	80

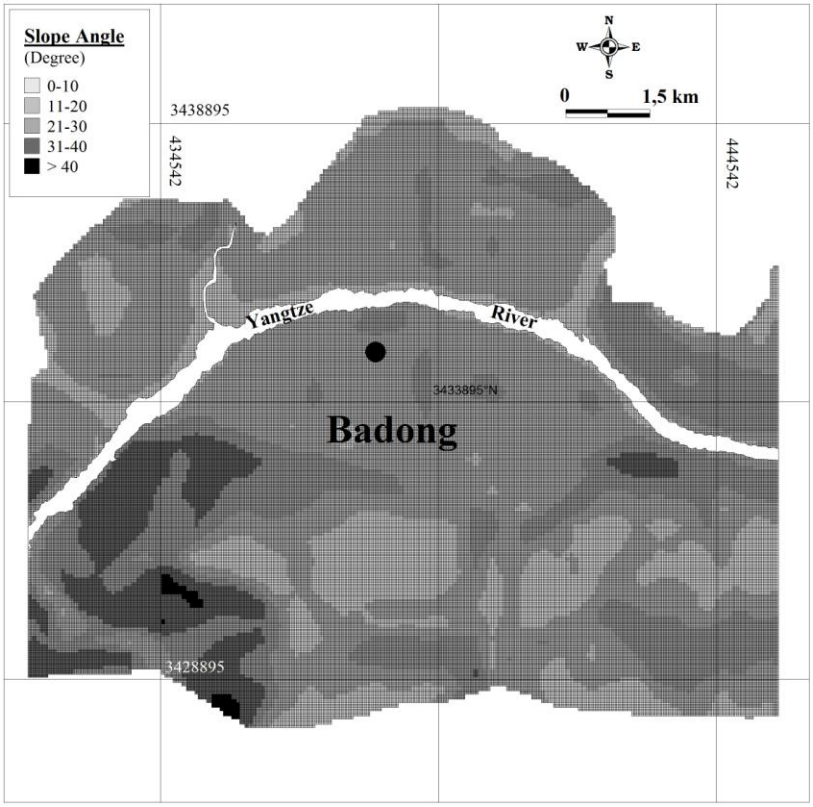

Figure 10. Thematic map prepared using the VGF file for slope angle.

Point scores (weighting factors) were given to the "slope angle" categories according to their landslide susceptibilities as follows: ten points for 0-10°; twenty points for 11–30°; and, thirty points for >31°, respectively.

Point scores (weighting factors) were given to the "slope aspect" categories according to their landslide susceptibilities with ten points for 45–90°, 90–135° and 225–270°, and twenty points for 0–45°, 135–180° and 180–225° slopes, respectively (Tables 3 and 4).

Point scores (weighting factors) were given to the "lithology" categories according to their landslide susceptibilities with ten points for bedded limestone, massive limestone and Presinian metamorphic and magmatic rocks, and thirty points for sandstone-shale-claystone intercalations.

Point scores (weighting factors) were given to the "lineament" and "drainage" categories according to their landslide susceptibilities as five, ten and fifteen for 0–50, 50–100 and 100–200 metres distance from the river bed, respectively.

Point scores (weighting factors) were given to the "vegetation" categories according to their landslide susceptibilities as ten points for the barren field, ten points for the less vegetation zones and zero-point for dense vegetation zones (Table 3).

Finally, all susceptibility point scores in the six columns were summed and a column named "Total" created in the database (Equation 1). The LSM was created as a thematic map based on the total value of these point scores after applying the relevant weighting factors.

76 ≤ Landslide Susceptibility => **High landslide susceptibility zone**

36 ≤ Landslide Susceptibility < 76 => **Moderate landslide susceptibility zone**

Landslide Susceptibility < 36 => **Low landslide susceptibility zone**

Classes were divided into three categories with the help of the landslide inventory map and statistical natural breaks of the total point range data (Figure 11).

The susceptibility of each 'vector pixel' to landslides is displayed in Figure 11 with an explanation of low to high landslide susceptibility. Areas of high susceptibility are categorised by steep slope gradients with a 'soft' sandstone-shale-claystone intercalations lithology. Smaller features with high susceptibility values observed in the map generally correspond to lineaments and/or drainage network. A LSM is considered to be categorised if it shows three susceptibility zones: (a) high, (b) moderate and (c) low landslide potential zones (Figure 11).

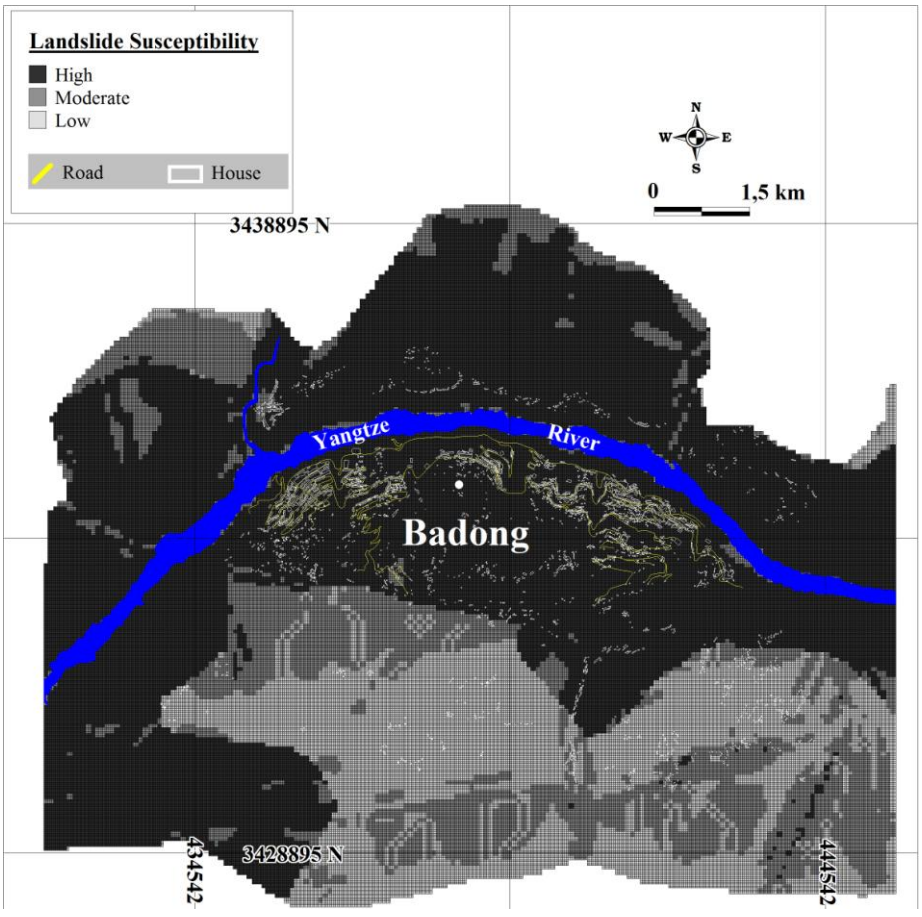

Figure 11. Landslide susceptibility map of the Badong County in the Three Gorges Region.

6. Validation of LSMs with PS InSAR Derived Deformation Map

Interferometric SAR (InSAR) has been used to map surface displacements of the Earth's surface by calculating the phase differences in complex representations (magnitude and phase). Synthetic Aperture Radar (SAR) images are acquired under similar geometric conditions but at different acquisition dates [73]. The sources of error for conventional InSAR principally include atmospheric water vapour effects and temporal decorrelation [74]. Several approaches have been developed to address these two issues. Ferretti et al. proposed Permanent Scatterers InSAR improved by Colesanti et al. and by Kampes [75–78]. In these methods, the amplitude information of a group of PS candidates are analysed using a series of interferograms. These methods work well in urban areas where corner-like reflecting objects appear bright in SAR images. But these methods do not turn out very well in natural terrain because of the absence of man-made structures [56]. The second approach identifies PS pixels primarily on phase characteristics as demonstrated by Hooper et al. [79,80]. This method can find low-amplitude but stable pixels that cannot normally be identified using only amplitude data.

Persistent Scatterer (PS) InSAR supports users with reliable deformation measurements by identifying single coherent pixels using a long temporal series of interferograms and estimating atmospheric signals [76].

In this study, the StaMPS package was used to process 13 ENVISAT images from descending track 075 collected between November 2003 and March 2008 [79]. The comparison between two adjacent tracks shows the PS derived deformation map is reliable with a RMS of 0.41 mm [56].

To evaluate the GIS-model, PS-InSAR derived deformation signals were overlaid on the susceptibility map. In Figure 10, grey points represent stable pixels, purple points indicate subsidence pixels and blue points imply uplift pixels. It should be noted that the density of PS-InSAR points does not show the magnitude of deformation; substantial clusters of PS-InSAR points merely correspond to more populated areas (e.g. houses indicated in white in Figure 12) which possibly exhibit high radar backscatter values from man-made buildings. A simple spatial analysis of Ikonos imagery reveals that 13.5 % of PS points are located on tops of buildings.

Although PS points are limited to points with good coherence from a long series of interferograms, there is a good correspondence of points with the GIS-based susceptibility model. It is clear in Tables 5 that 84.8% of the subsidence deformation points are located in areas classified by the GIS-model as moderately and highly susceptible to landslides.

Table 5. Distribution of the PS-point values to the landslide susceptibility classes.

Susceptibility / Deformation (mm/yr)	High	Moderate	Low	Total
0.6 to 4.2 (uplift)	85 (6.8%)	7 (0.6%)	17 (1.3%)	109 (8.7%)
-0.8 to 0.6 (stable)	187 (14.8%)	40 (3.2%)	38 (3.0%)	265 (21.0%)
-9.9 to -0.8 (subsidence)	615 (48.7%)	138 (10.9%)	135 (10.7%)	888 (70.3%)
Total	887 (70.3%)	185 (14.7%)	190 (15.0%)	1262 (100.0%)

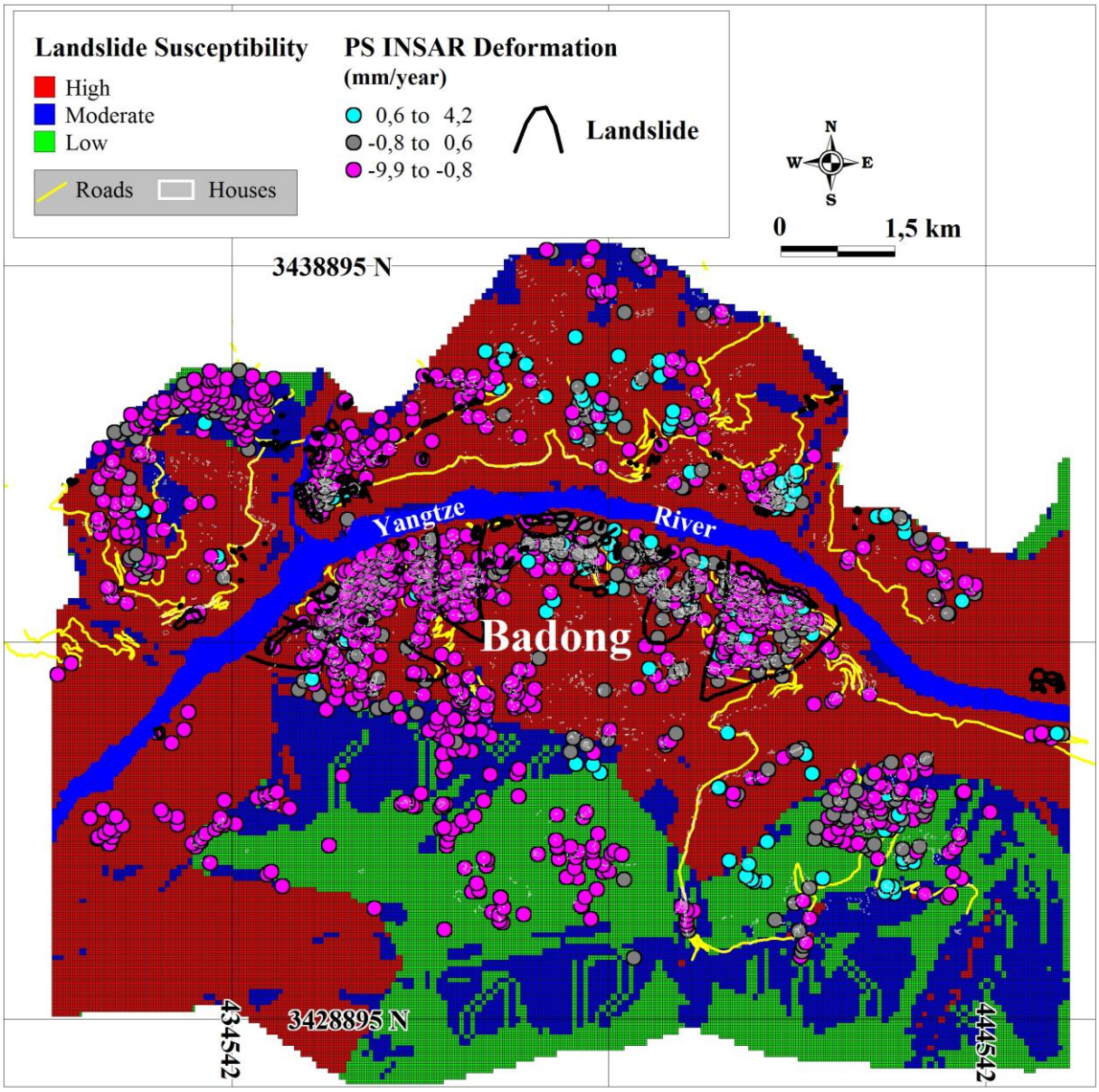

Figure 12. Landslide Susceptibility Map overlaid with PS InSAR derived deformation signals (Locations of the large landslides were extracted from [44]).

7. Conclusions

In this case study, a LSM generated for the Badong County, TG of China, using information layers derived from satellite optical images (specifically ASTER and Landsat) and ASTER GDEM, which agrees well with our PS InSAR derived deformation maps. Both suggest that 59.8% of the study area is classified as "Highly susceptible to landslides", and 19.4% of this is classified as "moderately susceptible to landslides" (Figure 12). 84.8% of the subsidence PS-InSAR points were calculated in moderately and highly susceptible landslide zone. Landslides which have occurred do indeed show in the "High landslide susceptibility zone" of the LSM prepared in this case study (Figure 13) [44].

A VGF was created to calculate a GIS-based analysis with 30 meters accuracy. For local scales, this resolution can be increased depending on the scales of the digital thematic maps prepared.

As a result, the investigated case study site of Badong County can be considered an active landslide area with the help of PS InSAR data and field observations. Landslides can be re-activated by the land-use changes which are now happening in Badong County. New landslides may occur in the area classified as "high landslide susceptible zone" in the LSM if preventive measures are not met against the triggering effect of reactivated fossil landslides. Mass movements, other than landslides, such as planar, wedge and toppling forms should also be analyzed in the future, after obtaining relevant detailed field data.

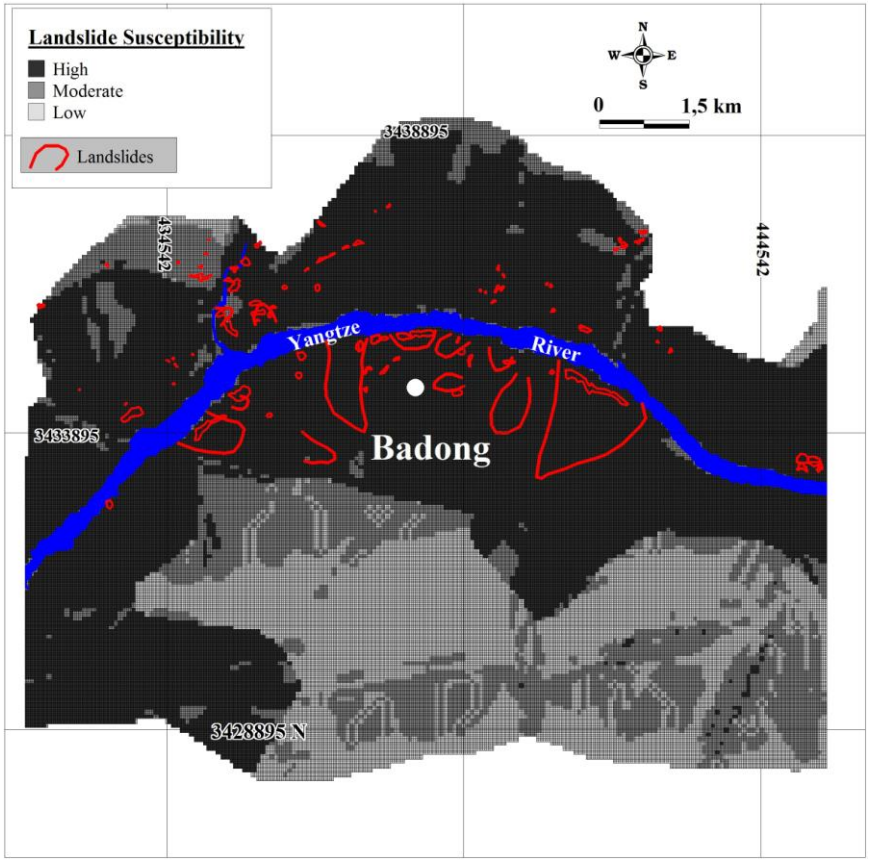

Figure 13. Landslides which were occurred previously as observed in the "High Landslide Susceptibility Zone" (Locations of the large landslides were taken from [44]).

Perspective

This work can be used in landslide susceptibility mapping studies if a vector-based database is available. Also, the weighting of each digital thematic layer on landslide susceptibility is scored in this case study. Authors who have score points for different geo-referenced areas could use this work in their studies. Vector-pixel based landslide susceptibility analyses has more advantages then raster-pixel based one. We suggest geoscientists to use this work in their scientific studies to obtain fast and reliable results during their landslide susceptibility analysis.

Acknowledgments

This work is supported by The Scientific and Technological Research Council of Turkey fellowship to CK and a CSC scholarship to PL. Part of this work is also supported by the Natural Environmental Research Council (NERC) through the GAS project (Ref: NE/H001085/1) as well as

by a China 863 Project (ID: 2009AA12Z317). The ENVISAT images were supplied through the ESA-MOST Dragon 2 Cooperation Program (ID: 5343, PI: J-P Muller).

Conflict of interest

All authors declare no conflicts of interest in this paper.

References

1. Wahono B.F.D. (2010) Applications of Statistical and Heuristic Methods for Landslide Susceptibility Assessments : A case study in Wadas Lintang Sub District Wonosobo Regency, Central Java Province, Indonesia, Graduate School, Faculty of Geography, Gadjah Mada University and International Institute for Geo-information Science and Earth Observation. p. 106.
2. Guzzetti F, Reichenbach P, Cardinali M, et al. (2005) Probabilistic landslide hazard assessment at the basin scale. *Geomorphol* 72: 272-299.
3. Chacon J, Irigaray C, Fernandez T, et al. (2006) Engineering geology maps: landslides and geographical information systems. *Bull Eng Geol Environ* 65: 341-411.
4. Radbruch DH (1970) Map of relative amounts of landslides in California, in US Geological Survey Open-File Report. p. 70-1485, 85-585.
5. Dobrovolny E (1971) Landslide susceptibility in and near anchorage as interpreted from topographic and geologic maps, in The Great Alaska Earthquake of 1964. *Natl Acad Sci* 735-745.
6. Nilsen TH and Wright RH (1979) Relative slope stability and landuse planning in the San Francisco Bay region, California. *Prof Pap* 103.
7. Brabb EE, Pampeyan EH, Bonilla MG (1972) Landslide Susceptibility in San Mateo County. California: U.S. Geological Survey. *Misc Field Stud Map* MF-360, Scale 1:62,500.
8. Carrara A, Cardinali M, Detti R, et al. (1991) GIS Techniques and Statistical-Models in Evaluating Landslide Hazard. *Earth Surf Processes Landforms* 16: 427-445.
9. Carrara A and Guzzetti F (1995) Geographical information systems in assessing natural hazards. *Springer Neth* 4: 45–59.
10. Chung CJF and Fabbri AG (1999) Probabilistic prediction models for landslide hazard mapping. *Photogramm Eng Remote* 65: 1389-1399.
11. Guzzetti F, Carrara A, Cardinali M, et al. (1999) Landslide hazard evaluation: a review of current techniques and their application in a multi-scale study, Central Italy. *Geomorphol* 31: 181-216.
12. Brabb EE (1993). Priorities for landslide during the international decade of hazard reduction. in Landslides : seventh international conference and field workshop. Rotterdam: Balkema.
13. Agostoni S, Laffi R, Mazzocola, et al. (1998). Landslide inventory data base for an Alpine area, Lombardia, Italy. in 8th IAEG Congress. Vancouver: A.A.Balkema.
14. Chau KT, Lo KH, (2004) Hazard assessment of debris flows for Leung King Estate of Hong Kong by incorporating GIS with numerical simulations. *Nat Hazards Earth Syst Sci* 4: 103-116.
15. Giardino M, Giordan D, Ambrogio S (2004) GIS technologies for data collection, management and visualization of large slope instabilities: two applications in the Western Italian Alps. *Nat Hazards Earth Syst Sci* 4: 197-211.
16. Lee S, Chwae U, Min KD (2002) Landslide susceptibility mapping by correlation between topography and geological structure: the Janghung area, Korea. *Geomorphol* 46: 149-162.
17. Lee S, Choi J, Min K (2002) Landslide susceptibility analysis and verification using the Bayesian probability model. *Environ Geol* 43: 120-131.

18. Süzen ML and Doyuran V (2004) A comparison of the GIS based landslide susceptibility assessment methods: multivariate versus bivariate. *Environ Geol* 45: 665-679.
19. Ermini L, Catani F, Casagli N (2005) Artificial Neural Networks applied to landslide susceptibility assessment. *Geomorphol* 66: 327-343.
20. Van Westen CJ, Van Ash TWJ, Soetoers R (2005) Landslide and risk zonation-why is it still so difficult? *Bull Eng Geol Env* 65: 167-184.
21. Magliulo P, Di Lisio A, Russo F, et al. (2008) Geomorphology and landslide susceptibility assessment using GIS and bivariate statistics: a case study in southern Italy. *Nat Hazards* 47: 411-435.
22. Kawabata D and Bandibas J (2009) Landslide susceptibility mapping using geological data, a DEM from ASTER images and an Artificial Neural Network (ANN). *Geomorphol* 113: 97-109.
23. Mejianavarro M, Wohl EE, Oaks SD (1994) Geological Hazards, Vulnerability, and Risk Assessment Using GIS - Model for Glenwood-Springs, Colorado. *Geomorphol* 10: 331-354.
24. Temesgen B, Mohammed MU, Korme T (2001) Natural hazard assessment using GIS and remote sensing methods, with particular reference to the landslides in the Wondogenet area, Ethiopia. *Phys Chem Earth Part C-Solar-Terrestial Planet Sci* 26: 665-675.
25. Zhu AX, Wang RX, Qiao JP, et al. (2004) Mapping landslide susceptibility in the Three Gorges area, China using GIS, expert knowledge and fuzzy logic. *IAHS Publ* 289: 385-391.
26. Kıncal C, Akgün A, Koca MY (2009) Landslide susceptibility assessment in the Izmir (West Anatolia,Turkey) city center and its near vicinity by the logistic regression method. *Environ Earth Sci* 59: 745–756.
27. Bai S-B, Wang J, Lü G-N, et al. (2010) GIS-based logistic regression for landslide susceptibility mapping of the Zhongxian segment in the Three Gorges area, China. *Geomorphol* 115, 23-31.
28. Yilmaz C, Topal T, Süzen ML (2012) GIS-based landslide susceptibility mapping using bivariate statistical analysis in Devrek (Zonguldak-Turkey) 65: 2161-2178.
29. Van Westen CJ (1993) Application of geographic information systems to landslide hazard zonation. *University Delft Inter Instit*.
30. Süzen ML and Doyuran V (2004) Data driven bivariate landslide susceptibility assessment using geographical information systems: a method and application to Asarsuyu cathment, Turkey. *Eng Geol* 71: 303-321.
31. Chen W, Li X, Wang Y, et al. (2013) Landslide susceptibility mapping using LIDAR and DMC data: a case study in the Three Gorges area, China. *Environ Earth Sci* 70:673-685.
32. Wu X, Niu R, Ren F, et al. (2013) Landslide susceptibility mapping using rough sets and back-propagation neural networks in the Three Gorges, China. *Environ Earth Sci* 70: 1307-1318.
33. Kavzaoglu T, Sahin EK, Colkesen I (2014) Landslide susceptibility mapping using GIS-based multi-criteria decision analysis, support vector machines, and logistic regression. *Landslides* 11:425-439.
34. Tehrany MS, Pradhan B, Jebur MN, (2014) Flood susceptibility ampping using a novel ensemble weights-of-evidence and support vector machine models in GIS. *J Hydrol* 512: 332-343.
35. Wu X, Ren F, Niu R (2014) Landslide susceptibility assessment using object mapping units, decision tree, and support vector machine models in the Three Gorges of China. *Environ Earth Sci* 71: 4725-4738.
36. Du W, Wu Y, Liu J, et al. (2016) Landslide Susceptibility Mapping Using Support Vector Machine Model. *Electron J Geotech Eng* 21: 7069-7084.
37. Li J and Yi C (2005) The Magnificent Three Gorges Project.

38. Fuggle R and Smith WT (2000) Experience with dams in water and energy resource development in the People's Republic of China, Cape Town (South Africa), Secretariat of the World Commission on Dams.
39. Liu JG, Mason PJ, Clerici N, et al. (2004) Landslide hazard assessment in the Three Gorges area of the Yangtze river using ASTER imagery: Zigui-Badong. *Geomorphol* 61: 171-187.
40. Boyle CE (2007) Water-borne Illness in China. China Environmental Health Project, Research Brief. Washington, D.C.: Woodrow Wilson International Center for Scholars.
41. Chinese Three Gorges Project Corporation (CTGPC), (2002) Flooding on the Yangtze in 1998. April 20, 2002. Retrieved on February 8, 2008. (Chinese).
42. Ministry of Environmental Protection The People's Republic of China (MOEPTPRCa), (2010) Three Gorges Bulletin in 2009 Chapter 2 Economic and Social Development 2010-02-23. Available from: http://english.mep.gov.cn/standards_reports/threegorgesbulletin/.
43. Ministry of Environmental Protection The People's Republic of China (MOEPTPRCb), (2010) Three Gorges Bulletin in 2009 Chapter 3, State of the Natural Ecological Environment 2010-02-23. Available from: http://english.mep.gov.cn/standards_reports/threegorgesbulletin/.
44. Wu S, Wang H, Han J, et al. (2009) The Application of Fractal Dimensions of Landslide Boundary Trace for Evaluation of Slope Instability, in Landslide Disaster Mitigation in Three Gorges Reservoir, China, T.L. Fawu Wang, Editor. Springer-Verlag: Berlin. 465-474.
45. Xue G, Xu F, Wu Y, et al. (2009) Bank Slope Stability Evaluation for the Purpose of Three Gorges Reservoir Dam Construction. *Springer Berl Heidelb* 41-86.
46. Wu SR, Shi L, Wang R, et al. (2001) Zonation of the landslide hazards in the for reservoir region of the Three Gorges Project on the Yangtze River. *Eng Geol* 59: 51-58.
47. Wu S, Hu D, Chen Q, et al. (1997) Assessment of the crustal stability in the Qingjiang river basin of the western Hubei Province and its peripheral area, China. in Thirtieth International Geological Congress. Beijing, China: VSP International Science Publishers.
48. Fourniadis IG and Liu JG (2007) Landslides in the Wushan-Zigui region of the Three Gorges, China. *Q J Eng Geol Hydrogeol* 40: 115-122.
49. METI/ERSDAC (2010) Earth Remote Sensing Data Analysis Center. 24 August 2010 16 June 2010]; METI/ERSDAC]. Available from: http://www.ersdac.or.jp/GDEM/E/4.html.
50. Stefanov WL, Ramsey MS, Christensen PR (2001) Monitoring urban land cover change: An expert system approach to land cover classification of semiarid to arid urban centers. *Remote Sens Environ* **77**: 173-185.
51. Zhu GB and Blumberg DG (2002) Classification using ASTER data and SVM algorithms; The case study of Beer Sheva, Israel. *Remote Sens Environ* 80: 233-240.
52. Stefanov WL and Netzband M (2005) Assessment of ASTER land cover and MODIS NDVI data at multiple scales for ecological characterization of an and urban center. *Remote Sens Environ* 99: 31-43.
53. U.S. Department of the Interior, U.S.G.S., (2010) USGS/EROS Find Data/Products and Data Available/ETM. 1 April 2010 [cited 2010 10 May 2010]; Available from: http://eros.usgs.gov/#/Find_Data/Products_and_Data_Available/ETM.
54. Irons JR (2010) The Landsat Program. National Aeronautics and Space Administration . 1 September 2010 [cited 2010 15 July 2010]; Available from: http://landsat.gsfc.nasa.gov/about/landsat7.html.
55. Li P, Shi C, Li Z, et al. (2013) Evaluation of ASTER GDEM using GPS benchmarks and SRTM in China. *Int J Remote Sens* 34: 1744-1771.

56. Liu P, Li Z, Hoey T, et al. (2011) Using advanced InSAR time series techniques to monitor landslide movements in Badong of the Three Gorges region, China. *Int J Appl Earth Obs Geoinform* 21: 253-264.
57. Dai FC, Lee CF, Li J, et al. (2001) Assessment of landslide susceptibility on the natural terrain of Lantau Island, Hong Kong. *Environ Geol* 40: 381-391.
58. Van Westen CJ, Rengers N, Soeters R (2003) Use of geomorphological information in indirect landslide susceptibility assessment. *Nat Hazards* 30: 399-419.
59. Ercanoglu M and Gokceoglu C (2004) Use of fuzzy relations to produce landslide susceptibility map of a landslide prone area (West Black Sea Region, Turkey). *Eng Geol*75: 229-250.
60. Ayenew T and Barbieri G (2005) Inventory of landslides and susceptibility mapping in the Dessie area, northern Ethiopia. *Eng Geol* **77**: 1-15.
61. Ayalew L and Yamagishi H (2005) The application of GIS-based logistic regression for landslide susceptibility mapping in the Kakuda-Yahiko Mountains, Central Japan. *Geomorphol* 65: 15-31.
62. Duman TY, Can T, Gökçeoğlu C, et al. (2006) Application of logistic regression for landslide susceptibility zoning of Cekmece Area, Istanbul, Turkey. *Environ Geol* 51: 241-256.
63. Fourniadis IG, Liu JG, Mason PJ (2007) Regional assessment of landslide impact in the Three Gorges area, China, using ASTER data: Wushan-Zigui. Landslides 4: 267-278.
64. Wang F and Li T (Eds.) (2009) Landslide Disaster Mitigation in Three Gorges Reservoir, China. *Mountain Res Dev* 30: 184-185.
65. E.R.S.D.A. (2010) About ASTER G-DEM. Available from: http://www.ersdac.or.jp/GDEM/E/1.html.
66. Kıncal C (2005) Engineering Geological Evaluation of Geological Units in and Around Izmir City Center with the Help of Geographical Information Systems and Remote Sensing Techniques, in The Graduate School of Natural and Applied Sciences. Dokuz Eylul University Izmir. p. 342.
67. Jimenez MJ, Fernandez MG, Zonno G, et al. (2000) Mapping soil effects in Barcelona, Spain, through an integrated GIS environment. *Soil Dyn Earthq Eng* 19: 289-301.
68. Kıncal C, Koca MY, van Loon AJ (2009) Large-scale land-suitability mapping in the GIS environment for the construction site of the University Olympic Village in Izmir (Turkey). *Geol* 15: 189-198.
69. Heywood DI, Cornelius S, Carver S (2006) An introduction to geographical information systems. 3rd ed., Harlow, England ; New York: Pearson Prentice Hall. xxxiii, 426 p.
70. Collins MG, Steiner FR, Rushman MJ (2001) Land-use suitability analysis in the United States: Historical development and promising technological achievements. *Environ Manage* 28: 611-621.
71. Sarkar S and Kanungo DP (2004) An integrated approach for landslide susceptibility mapping using remote sensing and GIS. *Photogramm Eng Remote Sens* 70: 617-625.
72. Pandy A, Dabral PP, Chowdary VM, et al. (2008) Landslide Hazard Zonation using Remote Sensing and GIS: a case study of Dikrong river basin, Arunachal Pradesh, India. *Environ Geol* 54: 1517-1529.
73. Massonnet D and Feigl KL (1998) Radar interferometry and its application to changes in the earth's surface. *Rev Geophys* 36: 441-500.
74. Hanssen RF (2001) Radar interferometry : data interpretation and error analysis. Remote sensing and digital image processing. Dordrecht ; Boston: Kluwer Academic. xviii, 308
75. Ferretti A, Prati C, Rocca F (2000) Nonlinear subsidence rate estimation using permanent scatterers in differential SAR interferometry. *Ieee Trans Geosci Remote Sens* 38: 2202-2212.

76. Ferretti A, Prati C, Rocca F, (2001) Permanent scatterers in SAR interferometry. *Ieee Trans Geosci Remote Sens* 39: 8-20.
77. Colesanti C, Ferretti A, Novali F, et al. (2003) SAR monitoring of progressive and seasonal ground deformation using the permanent scatterers technique. *Ieee Trans Geosci Remote Sens* 41: 1685-1701.
78. Kampes B (2005) Displacement Parameter Estimation using Permanent Scatterer Interferometry. *Delft Univ Technol* p. 168.
79. Hooper A, Zebker H, Segall P, et al. (2004) A new method for measuring deformation on volcanoes and other natural terrains using InSAR persistent scatterers. *Geophys Res Lett* 31**:** 5.
80. Hooper A, Segall P, Zebker H (2007) Persistent scatterer interferometric synthetic aperture radar for crustal deformation analysis, with application to Volcan Alcedo, Galapagos. *J Geophys Res-Solid Earth* 112: B07407.

AIMS Press

© 2017 Cem Kıncal, et al., licensee AIMS Press. This is an open access article distributed under the terms of the Creative Commons Attribution License (http://creativecommons.org/licenses/by/4.0)